2021

Enhancement of the Critical Heat Flux During the Cooling of Power Electronics

Yuyang Hu
Technische Universtät Dresden, Germany

Oliver Ziegler
Technische Universtät Dresden, Germany, oliver.ziegler@tu-dresden.de

Christiane Thomas
Technische Universtät Dresden, Germany

Ullrich Hesse
Technische Universtät Dresden, Germany

Stefan Wettengel
Technische Universtät Dresden, Germany

See next page for additional authors

Enhancement of the Critical Heat Flux During the Cooling of Power Electronics

Yuyang Hu[1], Oliver Ziegler[1]*, Stefan Wettengel[2], Christiane Thomas[1], Ullrich Hesse[1], Andreas Kluge[2], Lars Lindenmüller[2], Gerd Fischer[3]

[1] Bitzer-Chair of Refrigeration, Cryogenics and Compressor Technology, Technische Universität Dresden, Germany
Oliver.Ziegler@tu-dresden.de

[2] Chair of Power Electronics, Technische Universität Dresden, Germany
Stefan.Wettengel@tu-Dresden.de

[3] F&S Prozessautomation GmbH, Dresden, Germany
Gerd.Fischer@fs-aut.de

* Corresponding Author

ABSTRACT

Semiconductor-based power electronics such as IGBT (insulated-gate bipolar transistor) modules are used in various applications. During their operation, several kilowatts of waste heat are produced in a single module, which must be specifically dissipated in order to guarantee reliable operation. With the trend towards the downsizing of modules and the demand for high power density in the development of new IGBT-modules, there is a need for efficient heat dissipation.

Within the scope of a research project the principle of a natural circulation is investigated for the application of cooling power electronics referring to a patent of Fischer, Langebach and Lindenmüller (2017). A metal cover plate, a polycarbonate frame and the IGBT module form the experimental setup. The pool boiling of a low GWP refrigerant at the baseplate of the IGBT module is investigated. With the heat sink of the original base plate surface, a maximum heat flux of 88.6 kW/m² under certain conditions could be dissipated. This value is considerably lower than the results from literature. Additionally, various methods to improve the critical heat flux were conducted and the results are presented.

1. INTRODUCTION

IGBT-modules (insulated-gate bipolar transistor) are widely used in the control and conversion of electric power. With the development of the IGBT technology, the power density of IGBT modules is increased continuously in the last years, as shown in Figure 1. Correspondingly, the heat dissipation of IGBT modules is also increased significantly. There has been a demand for efficient heat sinks.

Figure 1: Development of power density of IGBT modules (Qian *et al.*, 2018)

The currently used heat sinks for IGBTs with high power density are mainly cold plates with integrated flow channels, where the heat transfer mechanism is based on single phase convection. The restrictions of the conventional cold plates are on the one side the relative low heat transfer coefficient (HTC) of single-phase convection and on the other side the uneven temperature distribution at the cooling surface. Besides, the cooling water for high voltage IGBT modules must be continuously deionized in order to prevent parasitic currents through the cooling water.

In this paper, a new heat sink using the concept of a vapor chamber is presented. The structure of the apparatus is described in 2.1. The main heat transfer mechanisms applied here are film condensation and pool boiling, which are characterized with HTC. Pool boiling is especially suitable for this application, since the HTC is increased with heat flux, which gives the heat sink the ability to damp peak loads as well as hotspots. However, the application of pool boiling is limited by the critical heat flux (CHF). As the CHF is reached, the liquid supply to the heated surface is not sufficient to replenish the vaporized liquid. Vapor blankets start to form at the surface, which leads to local dry-out and the surface temperature will increase dramatically. Since the temperature limit for silicon IGBTs is in the range of 125 °C to 175 °C, the boiling crisis could lead to burn-out of the power electronics.

Pool boiling as well as the enhancement of CHF have been extensively studied in literature. Forrest *et al.* (2013) measured the pool boiling CHF and HTC of Novec-649 (fluorinated ketone) on a circular aluminum surface at different saturated pressures. The experimental data were compared with the predicted results using available correlations. The Rohsenow correlation (Rohsenow, 1952) with the new fitted surface-fluid constant was shown to have the best prediction. Similarly, T'Jollyn *et al.* (2019) conducted pool boiling experiments of Novec-649 on a rectangular aluminum surface and compared the data with the results of several correlations. However, none of the correlations could predict the boiling curve accurately.

Because of the poor thermophysical properties, especially the low heat of evaporation and low surface tension, the CHF of the Novec-649 is much lower than that of water. In order to ensure a safe application of pool boiling with this dielectric coolant, it is of great interest to improve the CHF. There are basically two ways to enhance the CHF (Liang and Mudawar, 2019): (i). Modify the fluid properties and the operation conditions. (ii). Modify the boiling surface. This paper will focus on the methods of surface modification.

Kaniowski and Pastuszko (2018) experimentally investigated the boiling curve and HTC of Novec-649 on copper surfaces with open microchannels of different geometries. The CHF was shown to be improved with some of the tested geometries. Jaikumar and Kandlikar (2016) studied the enhancement effect of open microchannels on pool boiling of water by separating nucleation regions with feeder channels. The highest enhancement of the CHF was achieved when the width of the feeder channels was equal to the bubble departure diameter.

Sarangi *et al.* (2014) experimentally investigated the enhancement of pool boiling of FC-72 by laying free copper particles on the plain surface. With the copper particles of the size 45–53 µm, an improvement of 44% in CHF was obtained.

Yu and Lu (2007) conducted experiments with FC-72 on copper surfaces with rectangular fins of different geometries. The CHFs of the finned surfaces were higher than that of the plain surface. The enhancement increased with fin height and decreased with fin spacing.

In this paper, the pool boiling of Novec-649 on the base plate surface of a commercially available 4.5 kV IGBT module is experimentally investigated and several CHF enhancement methods are conducted. The test results are presented and discussed.

2. EXPERIMENTAL SETUP AND PROCEDURE

2.1 Experimental Setup

The structure of the heat sink is shown in figure 2. The heat sink consists mainly of four parts: a cover plate with an integrated fin-tube heat exchanger, a frame made of polycarbonate, a mounting plate and the IGBT module. Three O-rings are used for the sealing between these components. The components are fixed with threaded rods and thus form a sealed chamber. A dielectric refrigerant is filled in the chamber as the working medium. The refrigerant is heated by the IGBT module and pool boiling takes place at the surface of the IGBT's base plate. The produced refrigerant vapor is cooled by the heat exchanger at the top side of the chamber and the condensate drops back into the liquid pool. The boiling area on the base plate is 195 cm². The polycarbonate frame has a thickness of 40 mm and forms a vapor space of approximately (L x W x H) 185 x 150 x 80 mm. The cooling water for the condenser is supplied by a thermostat with a constant inlet temperature of 40 °C and a volume flow of 10 l/min. The refrigerant used here is Novec-649, which is nonflammable, nontoxic and environmentally friendly (GWP=1, ODP=0).

The chamber is put into a switch cabinet and connected with a cooling water supply, data acquisition and a power supply. All metal components are thermally insulated.

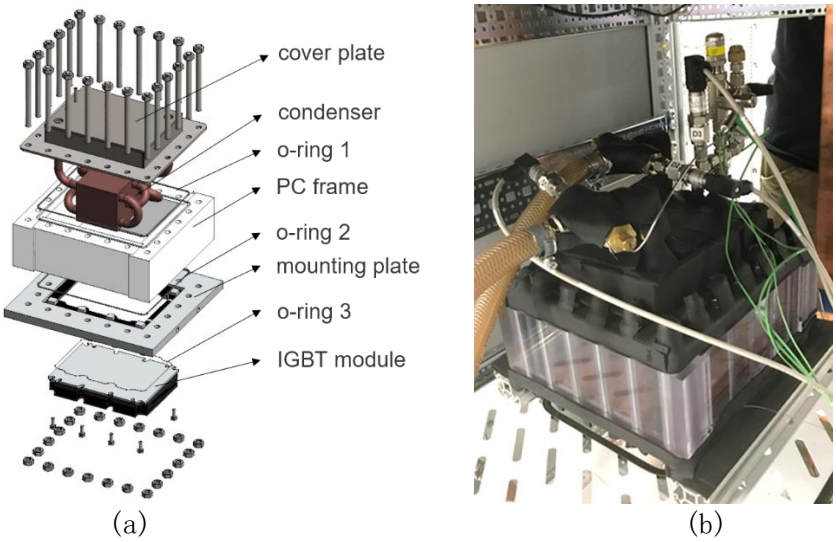

Figure 2: (a) 3D model of the structure and (b) a photograph of the "boiling cooler"

The measuring points of the temperatures and the pressures are presented in Figure 3. The temperatures (T1, T2) and pressures (P1, P2) of the cooling water are measured at the entrance and exit of the fin-tube heat exchanger, respectively. The volume flow of the cooling water is measured with an oval wheel flow meter. The pressure of the vapor chamber (P3) is measured at a measuring port located under the cover plate. The saturated temperature of the refrigerant is calculated from this pressure using the reference fluid properties database REFPROP 10 (Lemmon *et al.*, 2018). Four thermocouples are used to measure the base plate temperature, two of which (T3, T4) are located at midpoints of the long and the short side, respectively. The other two (T5, T6) are plugged into the IGBT module through two drilled holes at the enclosure and have direct contact with the back side of the base plate. The surface temperature of the cold plate is calculated from these four temperatures and is principally the average of the four

temperatures. (Remark: The internal thermocouples (T5 & T6) may not have very good thermal contact with the base plate as they are surrounded by silicone and therefore react more inertly compared to T3 & T4.)

The IGBT module is supplied with direct current (DC). The control signal (gate-emitter voltage) is provided by a battery and the IGBTs are maintained in switched on state. The heat output of the IGBT module is calculated using the collector-emitter voltage V_{CE} and collector-emitter current I_{CE}.

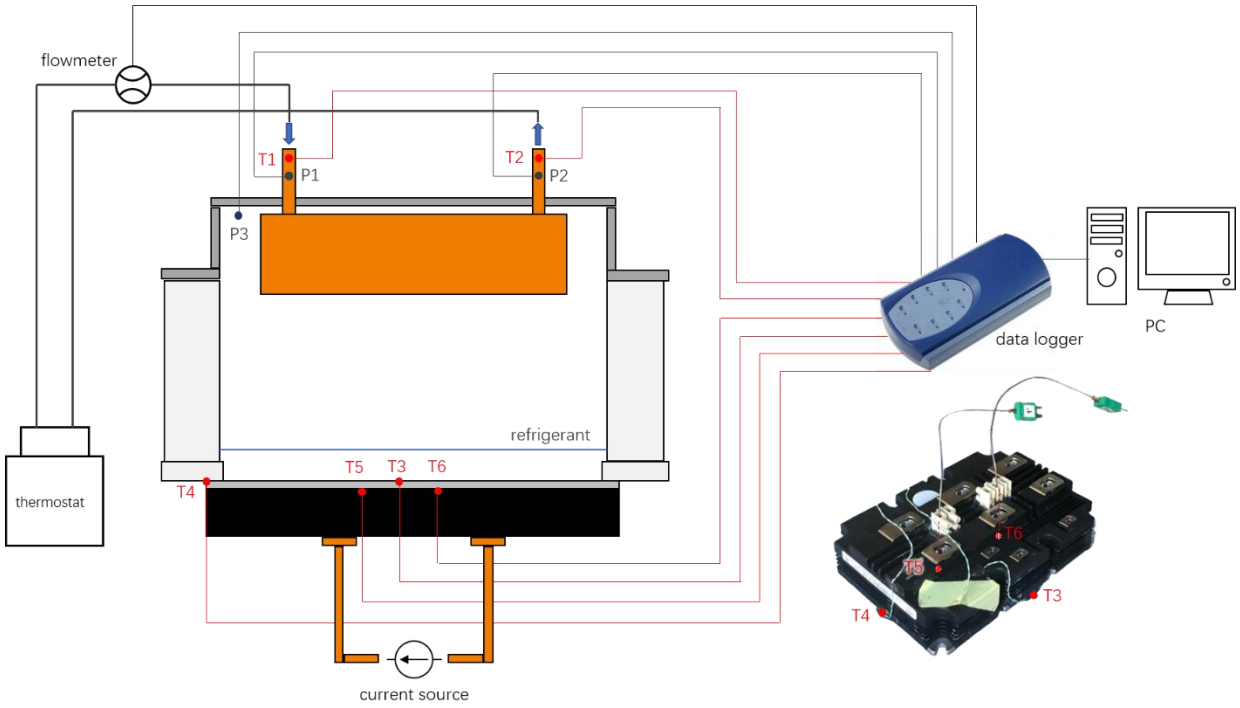

Figure 3: Measurement stand and the positions of the measuring points

2.2 Experimental Procedure

The chamber is evacuated using a vacuum pump before each experiment. A constant amount of refrigerant of about 150 ml is then filled in the chamber using a refrigerant cylinder. The thermostat and the IGBT module are then switched on. The inlet conditions of the cooling water are maintained constant. The power dissipation of the IGBT module is controlled by the DC power supply and is increased stepwise from a low value up to the CHF. Each step is maintained until the temperatures reach a steady state.

2.3 Methods to Enhance the Critical Heat Flux

During the experiment with the original "boiling-cooler" the CHF was reached. This was featured with the changes of the measured values and the bubble shapes. A sharp increase of the surface temperature T4 and a sudden drop of the vapor pressure P3 were recorded. A large vapor column was observed in the liquid pool. It must be noted that, due to the uneven distribution of the chips in the IGBT module, the heat flux on the surface of the base plate was not uniform and the CHF was firstly reached at some certain positions. The cooling capacity of the heat sink is limited due to CHF of the pool boiling. Efforts have been made to increase the CHF. Due to the restricted processing possibilities of the IGBT module itself the investigation focuses mainly on the effect of attachments on the original surface. The following variants were tested:

I). Silicon pin-fins

A silicon pin fin structure was constructed on the surface of the base plate, as shown in Figure 4. Because of the high process temperature, soldering or sintering with metals is not applicable for IGBT modules. In this case, a thermal adhesive is used as material for the pin-fin structure, which has a thermal conductivity of 0.2 $W \cdot (mK)^{-1}$. The spacing between two pin-fins is 2.5 mm. The diameter at the bottom and the height of each pin-fin is about 1.3 mm and 0.6 mm, respectively.

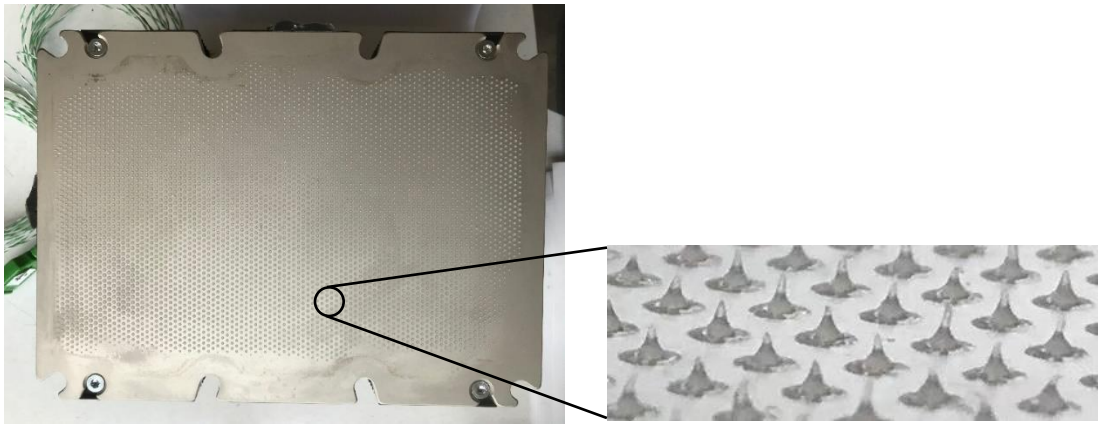

Figure 4: Base plate surface with silicon pin-fins

II). Free copper particles

Commercially available spherical copper particles with the diameters in the range of 37-88 μm were put on the surface of the base plate and then dispersed in the refrigerant. The copper powder was filtered using a sieve of 300 mesh into two variants with the size ranges of 37-50 μm and 50-88 μm, respectively. The amount of copper powder was selected to result in a powder layer with a thickness of four times the average diameter of the copper particles, which is considered as the optimal ratio for the heat transfer enhancement (Sarangi *et al.*, 2014).

III). Blind mounting plate with open microchannels

Instead of the mounting plate shown in Figure 2, a blind copper plate was used here as a mounting plate. The IGBT module is mounted on the one side of the copper plate with a graphite sheet as the thermal interface material. There is no direct contact of the base plate with the refrigerant, so that the boiling surface can be modified using common manufacturing processes. In order to increase the heat transfer area as well as to separate the flow paths of the replenishing liquid back to the boiling surface and the vapor escape channels, open microchannels are machined on the boiling surface. The geometry of the manufactured grooves is presented in Figure 5. The 0.7 mm pitch between two channels is equal to the capillary length of the Novec-649 at the corresponding saturated temperature of 65 °C, which is dependent on the thermal resistance of the condenser and the heat flux.

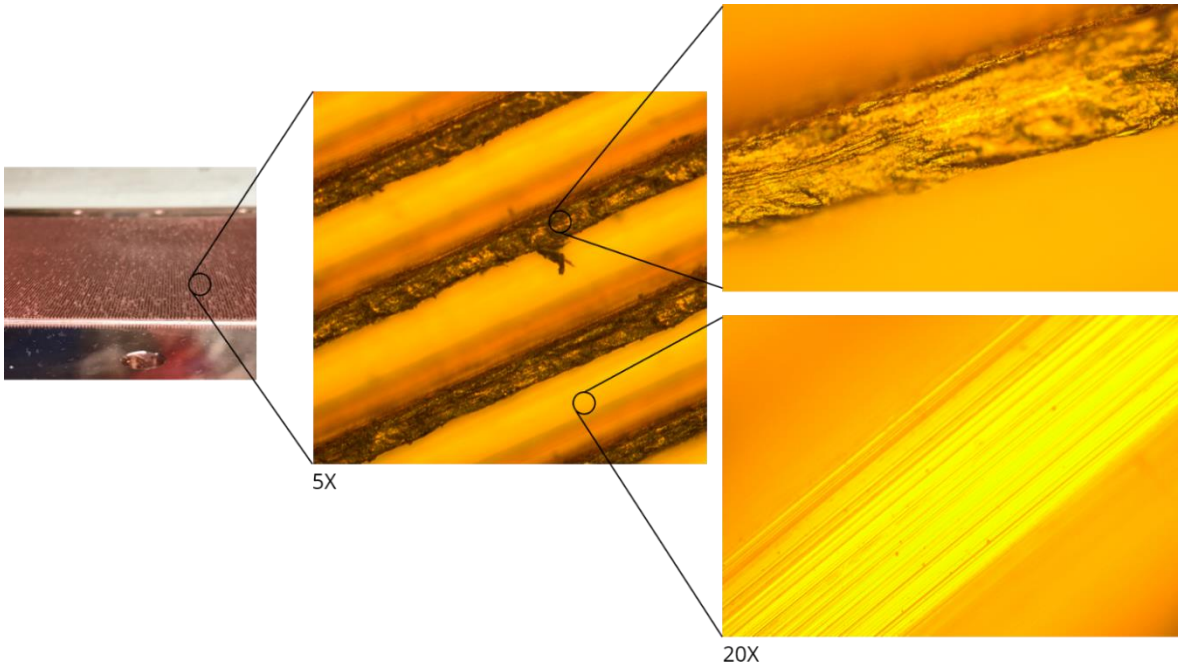

(a)

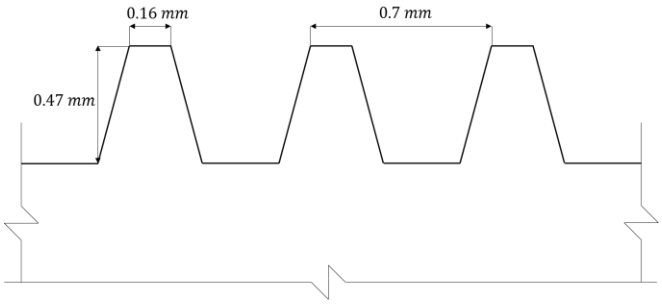

(b)

Figure 5: (a) Copper mounting plate with grooves on the boiling surface. (b) Side view of the grooves

3. DATA REDUCTION

To evaluate the cooling performance of the heat sink, the surface temperature of the base plate of the IGBT module and the heat flux are determined.

The heat dissipated by the heat sink is calculated using the following equation

$$\dot{Q} = \dot{V}_w \cdot \overline{\rho_w} \cdot \overline{C_{p,w}} \cdot (T_2 - T_1) \quad (1.)$$

where $\dot{V}_w$, $\overline{\rho_w}$, $\overline{C_{p,w}}$, T_2 and T_1 are the volume flow, the average density, the average heat capacity, the outlet and inlet temperature of the cooling water, respectively.

The average temperature of the boiling surface is calculated as follows:

$$T_s = \frac{1}{4} \cdot (T_3 + T_4 + T_5{}' + T_6{}') \quad (2.)$$

$$T_5{}' = T_5 - \frac{\dot{q} \cdot t}{\lambda_b} \quad (3.)$$

$$T_6{}' = T_6 - \frac{\dot{q} \cdot t}{\lambda_b} \quad (4.)$$

Here, $T_5{}'$ and $T_6{}'$ are the calculated temperatures at the heat transfer surface corresponding to the measuring points T_5 and T_6, $\dot{q}$ is the heat flux at the boiling surface, t is the thickness of the base plate and λ_b is the thermal conductivity of the base plate material.
The boiling heat transfer coefficient is calculated as

$$h = \frac{\dot{q}}{T_s - T_{sat}} \quad (5.)$$

The saturated temperature of the fluid T_{sat} is calculated from P1/P2 using REFPROP 10.

The uncertainties of the measured and calculated parameters are listed in Table 1. The error propagation is calculated with the method from Kline and McClintock (1953).

Table 1: Maximum uncertainty of the measured and calculated parameters

Parameters	Maximum uncertainty
T_1, T_2	$\pm$0.1 K
T_3, T_4, T_5, T_6	$\pm$2.6 K
T_s	$\pm$1.08 K
T_{sat}	$\pm$0.48 K
$\dot{q}$	$\pm$52.3%
h	$\pm$53.8%

4. RESULTS AND DISCUSSION

4.1 Heat Sink with the Original Base Plate

A "boiling curve" is presented in Figure 6 for the untreated surface of the base plate. Due to different heat fluxes and thermal resistances of the condenser, the saturated pressure in the heat sink grows with the heat flux. The "boiling curve" shows the relationship between the superheat temperature of the surface and the heat flux in an isochoric process. Because of the large uncertainties in the small heat flux range the curve only shows the measured points from a heat flux of 9.1 $kW \cdot m^{-2}$.

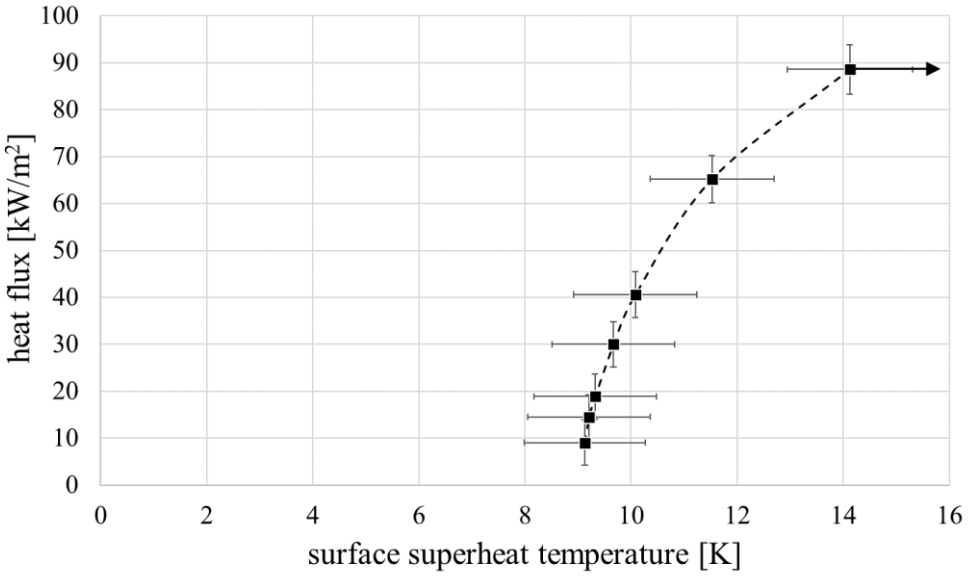

Figure 6: Dependence of the heat flux on the surface superheat temperature
(Lines are for illustration purposes only and do not represent interpolation.)

In the small heat flux range, the heat transfer is achieved by means of free convection and fluctuations of the liquid surface are observed. With enhanced heat flux, a large bubble column suddenly appears at one certain position of the base plate without transition. Increasing the heat flux further, another two bubble columns are seen in the liquid pool. After that, the other nucleation sites are activated and the boiling spreads over the complete surface. There are mainly two reasons for the sudden and unequally distributed boiling incipience: (1). The dielectric refrigerant has a small contact angle and will penetrate in the surface cavities, which reduces the size of the vapor embryo in the cavity and thus increases the required surface superheat to initiate nucleate boiling, as described in Liang and Mudawar (2019). (2). The heat flow is unevenly distributed among the surface of the base plate. The incipience of boiling is easier at the hotspots.

The boiling crisis occurs at a relatively high heat flux. At this heat flux, the pressure of the vapor chamber suddenly drops due to the deterioration of the vapor generation or the boiling heat transfer. At the same time the measured surface temperatures increase dramatically. The power supply is switched off immediately to protect the IGBT module. The CHF in this case is measured to be 88.6 $kW \cdot m^{-2}$ at a saturated pressure of 1.54 bar. This value is much lower than the prediction of 157.1 $kW \cdot m^{-2}$ with the Zuber-Kutateladze correlation, which can be found in Arik *et al.* (2011). Compared with results in the literature, such as Forrest *et al.* (2013) and T'Jollyn *et al.* (2019), this value is considerably lower. This is due to the uneven distribution of the heat flux at the boiling surface and the whole surface is thus in different nucleate boiling regions. As one hotspot reaches the CHF condition locally, the other areas are still in the nucleate boiling region. The size and thickness of the heated plate should have less effect, since the non-dimensional characteristic length L' and the thermal activity parameter S in all three experiments are well beyond the asymptotic limits according to Arik *et al.* (2011). The temperature difference across the base plate shortly before reaching the CHF is shown to be at least 17 K.

4.2 Base Plate with Attachments

The dependency of heat flux on the surface superheat temperature for the cases described in 2.3 is presented In Figure 7. Enhancement of the CHF is achieved with the silicon pin-fins, the free copper particles with the size 37-50 μm and the copper plate with open microchannels.

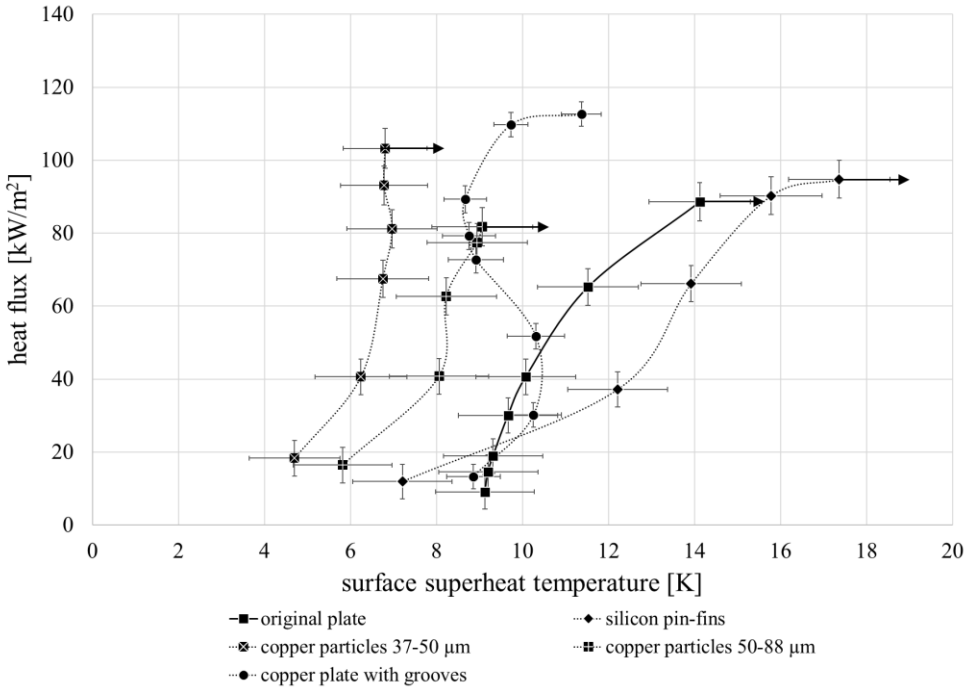

Figure 7: Heat flux versus surface superheat temperature of the methods tried to enhance the CHF (Lines are for illustration purposes only and do not represent interpolation.)

(1). Silicon Pin-fins

It can be seen from Figure 7 that the boiling heat transfer coefficient for the surface with silicon mini-pin-fins is lower than the original smooth surface at most heat fluxes. This is due to the low thermal conductivity of the silicon adhesive. About 25% of the complete surface area is covered with silicon adhesive. The surface temperature of the silicon pin-fins is much lower than that of the base plate. When the base plate surface is in the region of nucleate boiling, the dominant phenomenon on the pin-fin surface is still single-phase convection, which has a much lower HTC than nucleate boiling.

The CHF of this variant is shown to be a little higher than the original surface, but the enhancement of about 7 % lies in the area of uncertainty. The possible enhancement might be explained with two reasons: (i). The activation of nucleation sites on the pin-fins at high surface superheat, as the base plate surface enters the transition boiling region. (ii). The pin-fins could maintain flow channels for the liquid replenishment to the base plate surface.

(2). Free copper particles

Both variants with copper particles show an increase of the HTC compared with the original bare surface. The reason is the increase of nucleation site density, as the copper particles form extra cavities between particles and the plain surface and between the particles themselves which are suitable for bubble nucleation.

The larger particles with the size of 50-80 μm tend to remain at the surface. This leads to formation of a relatively thick layer of particles at the surface, which is good for increasing the number of nucleation sites, but unfavorable for the bubble departure and liquid replenishment. In the experiment, a kind of local “explosion” can be seen as a result of vapor accumulation in the particle layer and sudden release at a sufficient vapor pressure. Correspondingly, the HTC is enhanced significantly but the CHF is decreased compared with the original surface.

The smaller copper particles with the diameter range of 37-50 μm tend to suspend more evenly in the liquid. The particle layer on the surface is thinner than that of the large particles with diameter of 50-80 μm. As a result, the CHF

in this case is higher than that with larger copper particles. Compared with the original surface, the CHF with the smaller copper particles is 16% higher. The reasons could be: (i). The copper particles remained on the surface may introduce capillary effect, which reinforces the liquid supply to the nucleation sites. In Figure 8 small holes with diameters in the range of 0.6 mm to 0.9 mm can be seen in the particle layer, which are considered to be active nucleation sites. The copper particles surround them may form continuous liquid supply channels through capillary wicking. The large patches are believed to be formed by the vapor mushrooms near the CHF. Due to discharge of the refrigerant the particles accumulate in front of the drain port. (ii). The surface could be roughened through the collision of the suspended copper particles, as described in Sarangi *et al*. (2014).

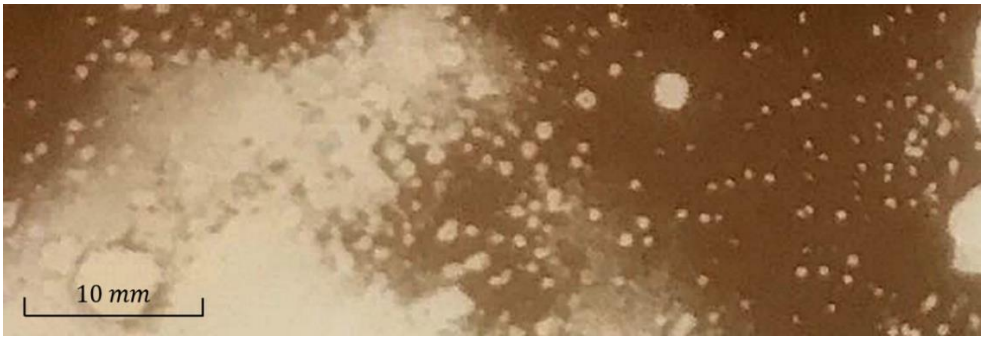

Figure 8: Top view of the base plate surface covered with a layer of copper particles after experiment

(3). Blind mounting plate with open microchannels

The copper plate with open microchannels is shown to increase both HTC and CHF. The CHF condition was not reached due to the temperature limitation of the IGBT module. With the tested highest heat flux, the CHF on the projected surface of copper plate is at least 27% higher than the original surface of the base plate. The boiling incipience happens at various sites on the surface of the copper plate with small bubble jets. The bubbles remain isolated from each other even at high heat flux. The enhancement is attributed to three reasons: (i). The enhancement of the heat transfer area. (ii). The heat spread in the copper plate reduces the temperature at the hotspots. The heat flux is more evenly distributed among the heat transfer area. (iii). Because of the manufacturing process the fin tops have much rougher surfaces than the microchannels, as can be seen in Figure 5. There are more potential nucleation sites at the fin top and bubbles are expected to be generated at the fin tops, even though the temperatures at the fin tops are lower than those at bottoms of the microchannels. The surfaces in the grooves remain flooded with liquid. The paths for bubble departure and for liquid replenishment are thus separated. The liquid supply to the nucleation sites is improved and this leads to the enhancement of CHF.

5. CONCLUSIONS AND OUTLOOK

A heat sink concept for IGBT modules with the principle of natural circulation was presented. Pool boiling of the coolant Novec-649 directly on the surface of the base plate of an IGBT module was experimentally investigated. Several potential methods to increase the CHF of the heat sink were tested, including silicon pin-fins directly adhered to the surface, free copper particles and a mounting plate with open microchannels. The conclusions are as follows:

- The pool boiling CHF of Novec-649 on the base plate of an IGBT module is much lower than the literature values, which are obtained on boiling surfaces with uniformly distributed heat flux.
- A kind of pin-fins made of silicon adhesive reduce the HTC and increase the CHF potentially. The reason for the heat transfer degradation is the low thermal conductivity.
- Free copper particles increase the HTC of pool boiling. The particles with the diameter of 37-50 μm increase the CHF by 16%, compared with the original bare surface.
- The HTC and CHF of pool boiling on the copper surface with grooves are considerably higher than those on the base plate.

In further investigations, the boiling cooler will be renewed and a more efficient condenser will be used. It is assumed that this is an additional reason for the significantly lower values of CHF than found in the literature. In addition, an easy-to-manufacture concept with a base plate made of copper and different surface treatment methods is pursued. The results will be presented in future publications.

NOMENCLATURE

T1…T6	measured temperatures	(K)
T_s	average surface temperature	(K)
T_5', T_6'	calculated surface temperature	(K)
T_{sat}	saturated temperature	(K)
P1… P3	measured pressures	(bar)
V_{CE}	collector-emitter voltage	(V)
I_{CE}	collector-emitter current	(A)
$\dot{Q}$	heat dissipation	(W)
$\dot{V}_w$	volume flow of cooling water	(m^3/s)
$\overline{\rho_w}$	average density of water	(kg/m^3)
$\overline{C_{p,w}}$	average specific heat of water	$(\mathrm{J}/(\mathrm{kgK}))$
$\dot{q}$	heat flux	(W/m^2)
h	heat transfer coefficient	$(\mathrm{W}/(m^2K))$

GWP	global warming potential	HTC	heat transfer coefficient
ODP	ozone depletion potential	CHF	critical heat flux

REFERENCES

Fischer, G., Langebach, R., Lindenmüller, L. (2017). Patent: *Kühlkörper mit zwei Hohlkörpern und Kühlanordnung* https://depatisnet.dpma.de/DepatisNet/depatisnet?action=bibdat&docid=DE102017215952B3, Germany

Qian, C., Gheitaghy, A. M., Fan, J.J., Tang H., Sun, B., Ye, H., Zhang, G. (2018). Thermal Management on IGBT Power Electronic Devices and Modules. *IEEE Access, volume 6*, 12868–12884.

Forrest, E. C., Hu, L., Buongiorno, J., McKrell, T. J. (2013). Pool Boiling Heat Transfer Performance of a Dielectric Fluid with Low Global Warming Potential. *Heat Transfer Engineering, 34(15)*, 1262-1277.

T'Jollyn, I., Nonneman, J., De Paepe, M. (2019). Pool boiling heat transfer measurements on a horizontal plate with a low global warming potential refrigerant. B1: Thermodynamics & Transfer Processes, Efficient Heat and Mass Transfer Processes (9), *The 25th IIR International Congress of Refrigeration*. Montréal, Québec, Canada, IIF/IIR.

Liang, G., Mudawar I. (2019). Review of pool boiling enhancement by surface modification. *International Journal of Heat and Mass Transfer, 128 (2019)*, 892–933.

Rohsenow W.M. (1952). A method of correlating heat transfer data for surface boiling of liquids. *Transactions of the ASME 74*, 969–976

Kaniowski1, R., Pastuszko, R. (2018). Boiling of a refrigerant of low GWP on the surface with copper microchannels. *E3S Web of Conferences 70*, 02007(2018).

Jaikuma, A., Kandlikar, S. G. (2016). Pool boiling enhancement through bubble induced convective liquid flow in feeder microchannels. *Applied Physics Letters 108*, 041604 (2016).

Sarangi, S., Weibel, J. A., Garimella, S. V. (2015). Effect of particle size on surface-coating enhancement of pool boiling heat transfer. *International Journal of Heat and Mass Transfer*, 81 (2015), 103–113.

Yu, C. K., Lu, D. C. (2007). Pool boiling heat transfer on horizontal rectangular fin array in saturated FC-72. *International Journal of Heat and Mass Transfer*, 50 (2007), 3624–3637.

Lemmon, E.W., Bell, I.H., Huber, M.L., McLinden, M.O. (2018). NIST Standard Reference Database 23: Reference Fluid Thermodynamic and Transport Properties-REFPROP, Version 10.0, *National Institute of Standards and Technology, Standard Reference Data Program*, Gaithersburg, 2018.

Kline, S. J. McClintock, F. A. (1953). Describing uncertainties in single-sample experiments. *Mechanical Engineering*, Vol. 75, 1953. 3-8.

Arik, M., Kosar, A., Bostanci, H., Bar-Cohen, A. (2011). Pool Boiling Critical Heat Flux in Dielectric Liquids and Nanofluids. *Advances in Heat Transfer*, vol. 43, 1-76.

ACKNOWLEDGEMENT

The authors acknowledge the financial support provided by die Sächsische Aufbaubank - Förderbank - (SAB).